19. C. H. Bennett, in *Diffusion in Solids: Recent Developments*, A. S. Nowick and J. J. Burton, Eds. (Academic Press, New York, 1975), pp. 73–113; D. Chandler, *J. Chem. Phys.* **68**, 2959 (1978).
20. See, for example, K. F. Kelton, in *Crystal Nucleation in Liquids and Glasses*, H. Ehrenreich and D. Turnbull, Eds. (Academic Press, Boston, 1991), vol. 45, pp. 75–177. As shown in this reference, the constant of proportionality is system-specific.
21. G. M. Torrie and J. P. Valleau, *Chem. Phys. Lett.* **28**, 578 (1974).
22. C. Haas and J. Drenth, *J. Cryst. Growth* **154**, 126 (1995).
23. A. J. Malkin and A. McPherson, *ibid.* **128**, 1232 (1992); *ibid.* **133**, 29 (1993).
24. J. P. Hansen and L. Verlet, *Phys. Rev.* **184**, 151 (1969).
25. We thank E. J. Meijer for computing part of the phase diagram in Fig. 1B, and A. van Blaaderen, M. Dogterom, J. Drenth, J. M. W. Frenken, S. Fraden, C. Haas, H. N. W. Lekkerkerker, B. Smit, R. Sear, J. T. M. Walraven, and C. Zukoski for critical reading of the manuscript. Supported by Scheikundig Onderzoek Nederland and by Fundamenteel Onderzoek der Materie (FOM) with financial aid from Nederlandse Organisatie voor Wetenschappelijk Onderzoek. Computer time was provided by Nationale Computer Faciliteiten.

9 June 1997; accepted 11 August 1997

Reversible Tuning of Silver Quantum Dot Monolayers Through the Metal-Insulator Transition

C. P. Collier, R. J. Saykally, J. J. Shiang, S. E. Henrichs, J. R. Heath*

The linear and nonlinear ($\chi^{(2)}$) optical responses of Langmuir monolayers of organically functionalized silver quantum dots were measured as a continuous function of interparticle separation under near-ambient conditions. As the distance between metal surfaces was decreased from 12 to ~5 angstroms, both quantum and classical effects were observed in the optical signals. When the separation was less than 5 angstroms, the optical second-harmonic generation (SHG) response exhibited a sharp discontinuity, and the linear reflectance and absorbance began to resemble those of a thin metallic film, indicating that an insulator-to-metal transition occurred. This transition was reversible.

Recent developments in chemical techniques for producing narrow size distributions of various metal (*1*) and semiconductor (*2–4*) quantum dots, and for fabricating ordered superlattices from these nanocrystals, have sparked much interest in the possibility of forming solids that have electrical and optical properties that could be tuned through chemical control over particle size, stoichiometry, and interparticle separation (*5–10*). In principle, control over interparticle separation provides a means for controlling both quantum and classical coupling interactions. This is of practical importance because control of quantum interactions would provide a route to preparing a solid of quantum dot "atoms" and precisely tuning the electronic properties of that solid by controlling the wave function overlap between adjacent particles. Although recent reports have documented classical (energy-transfer) coupling (*11, 12*) between semiconductor quantum dots (*13, 14*), quantum coupling has not been observed. Nor has quantum coupling been documented in coinage metal quantum dots, even though classical coupling [in the form of color changes (*15*)] and percolation phenomena (*16*) have long been observed in such systems.

Here, we describe in situ measurements of both the linear and nonlinear optical properties of organically functionalized silver nanocrystal Langmuir monolayers as a continuous function of interparticle separation distance. As the monolayer is compressed from an average separation between the surfaces of the metal cores (δ) of 12 ($\pm$2) Å to ~5 ($\pm$2) Å, the linear and nonlinear optical properties reveal evidence of both classical and quantum interparticle coupling phenomena. Below $\delta \sim 5$ Å, evidence for a sharp insulator-to-metal transition is observed in both optical signals. The nonlinear optical response abruptly decreases to a nearly constant value, and the linear reflectance drops precipitously until it matches that of a continuous metallic film. This transition is reversible: The particles can be redissolved (as a colloid), or, if the trough barriers are opened, the film is again characterized by the optical properties of near-isolated silver nanocrystals.

Silver quantum dots are expected to exhibit strong linear and nonlinear optical responses (*17*). The linear response is dominated by the surface plasmon resonance ω_{sp}. This transition, which has no molecular analog, is characterized by an oscillator strength resembling the physical dimensions of the particle (*18*). ω_{sp} can be modeled as the free (valence) electrons in the particle responding to an applied electromagnetic field, with the positive nuclear cores providing a restoring potential. For particles in the size range considered here (2 to 5 nm), ω_{sp} is determined by the free electron density in the particle and by the dielectric surrounding the particle surface. The resonance width is determined by the time scale for electron scattering at the particle boundaries and is dependent on particle size. The physical picture describing the nonlinear optical response is somewhat different. Consider an electron cloud associated with a nanoparticle. $\chi^{(1)}$ is a measurement of the polarizability of the cloud, which scales as the volume of the particle. $\chi^{(2)}$, the second-order susceptibility, is a measurement of how $\chi^{(1)}$ changes with respect to an applied electric field. A requirement for a nonzero $\chi^{(2)}$ is a lack of inversion symmetry, a condition that is met by a supported monolayer of nanocrystals. $\chi^{(2)}$ is almost exclusively sensitive only to the optical response of the crystallites and is a near background-free measurement.

Both the linear and nonlinear optical responses should provide excellent probes of interparticle coupling. When particles are brought into close proximity to one another, the dielectric surrounding a single particle is strongly modified by the presence of adjacent (conducting) spheres, resulting in shifts (to lower energy) of ω_{sp}. For quantum mechanical coupling, delocalization of charge carriers over multiple particles increases the scattering lifetime and leads to narrower plasmon linewidths. In the limiting case of complete electron delocalization between particles (that is, the formation of a continuous metal film), strong carrier absorption at energies below ω_{sp} and low reflectivity are expected. For example, consider the familiar case of thin metal films, which tend to be darkly colored. Only when a metal film is substantially thicker than the optical skin depth does it become reflective.

$\chi^{(2)}$ should also be an excellent probe of interparticle coupling. A nonlinear optical response is enhanced if the resonant state has both high oscillator strength and large volume (*19–21*), criteria that are satisfied by the particles discussed here. For classical coupling, local field effects should modify $\chi^{(2)}$ according to multipole coupling models (*22*). In contrast, quantum mechanical cou-

C. P. Collier and R. J. Saykally, Department of Chemistry, University of California, Berkeley, CA 94720, USA.
J. J. Shiang, S. E. Henrichs, J. R. Heath, Department of Chemistry and Biochemistry, University of California, 405 Hilgard Avenue, Los Angeles, CA 90095, USA.
*To whom correspondence should be addressed.

pling requires finite electron density to exist between adjacent crystallite (positive) cores. Electron density models predict appreciable free-electron density beyond the hard sphere boundary of coinage and alkali metal particles (*23*), making them excellent candidates for observing quantum mechanical coupling. As nanocrystals are brought close together, an increasing charge density builds up between the particles. This charge density is well shielded from the positive cores and is then more susceptible to the electric field gradients applied by incident laser beams.

Such experiments require particles that can form quasi-ordered monolayers on water and have sufficient compressibility to allow a range of interparticle separations. We used alkylthiol-capped silver nanocrystals (*24*); these particles are soluble in nonpolar organics, and the dominant interparticle interactions are attractive dispersion forces (*5*). Several Ag particle size–ligand combinations were used, and we labeled them according to the size of the metal core and the number of carbon atoms in the linear alkyl thiol that passivates the surface. For example, 27 Å silver cores capped with hexanethiol are denoted 27 Å/C_6. All particles are characterized by a size distribution width of $\sim \pm 10\%$. Most of the data discussed here were obtained from 27 Å/C_{10}, 27 Å/C_6, and 40 Å/C_3 particles. The pressure (π)–temperature (T) phase diagrams of Langmuir monolayers of similar particles have been reported previously (*24*). In a phase diagram corresponding to particles with properties similar to those used here (Fig. 1), the highly compressible "gas" phase consists of a microscopic structure of particle islands and voids on the water surface. The pressure range between the gas phase and the collapsed monolayer phase corresponds to the region in which the interparticle separation distance is changing. Note the negative $d\pi/dT$ slope of the boundary between the two-dimensional (2D) and collapsed 2D phases, which implies an entropy increase across the boundary. This is confirmed by observations: The collapsed (bi)layer is disordered, whereas the monolayers have some order, with domain sizes ranging from 0.1 to 1 μm^2. At lower temperatures, higher pressure is required to collapse the 2D phase, and the interparticle separation distance at the phase boundary is reduced. Thus, all experiments were carried out at 15°C.

All particles form strongly colored, clear yellow colloids. Because the particles are characterized by a strong optical resonance, a single monolayer is readily observed by eye. The gas phase has the appearance of a lightly hued, transparent film. For the 27 Å/C_{10} and 27 Å/C_6 particles, the monolayer film is orange to red in color, and for the 40 Å/C_3 particles, it is purple (these optical properties are explained below). Upon compression, the 2D phase takes on the appearance of a continuous, shiny film. Upon collapse, 2D–collapsed 2D phase boundaries appear parallel to the mobile barriers of the Langmuir trough. Particle films, complete with phase boundaries and other density gradients, can be lifted off intact as Langmuir-Schaeffer films, and particle sizes and separation distances can then be characterized by transmission electron microscopy (TEM) (Fig. 2) (*25*). The 40 Å/C_3 films were not sufficiently stable to allow for TEM imaging (*26*), and interparticle separation distances for those films were estimated from the optical properties, the monolayer densities, and basic chemical considerations. Although the 40 Å/C_3 particles are not particularly stable, high-quality films can be prepared from freshly synthesized particles.

Several measurements could be carried out simultaneously as a particle film was compressed on the Langmuir trough: the surface pressure of the film (as π-area isotherms), linear reflectance or absorbance, and the second-harmonic generation (SHG) response. Thirty reflectance spectra (from 1.5 to 3.5 eV) were collected, one every 12 s, during a compression cycle. A white light source was reflected from the surface of the Langmuir film and dispersed through a monochromator onto a diode array detector. For absorbance measurements, the white light was reflected from a submerged mirror. The SHG signal was measured by reflecting a 5-μJ, 50-ps pulse of s-polarized 1064-nm radiation from the monolayer (spot size, 1 mm). Laser fluences were reduced to prevent monolayer damage (*27*). Optical and polarization filters were inserted in the beam path to measure polarization information and to make certain that only 1064-nm radiation was incident on, and only 532-nm radiation was collected from, the film surface. A fraction of the 1064-nm laser beam was directed through a potassium dihydrogen phosphate (KDP) crystal, and the resulting SHG signal was used to normalize for single-shot power fluctuations. The point-to-point stability of a 10-point averaged SHG signal on a static sample was better than 10%. Because of the strong overlap of ω_{sp} with 532 nm, an SHG signal was readily obtained from the uncompressed monolayer.

Two signals were monitored as a function of area per particle for the 27 Å/C_6 particles: the surface pressure of the Langmuir film (π) and the enhancement of the p-polarized SHG (Fig. 3A). The SHG was normalized to the (nonzero) signal observed for an uncompressed monolayer, such that

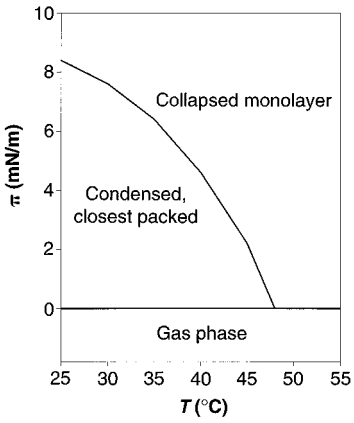

Fig. 1. Surface pressure (π) versus temperature (T) phase diagram for closest-packing Langmuir monolayers of organically passivated metallic nanocrystals similar to those used here, adapted from (*24*). The pressure range labeled "condensed, closest packed" corresponds to the region in which interparticle distance is changing in the 2D monolayer. At lower temperatures, compression of the monolayer provides a larger dynamic range of particle-particle separation distances and closer ultimate interparticle separation just before monolayer collapse.

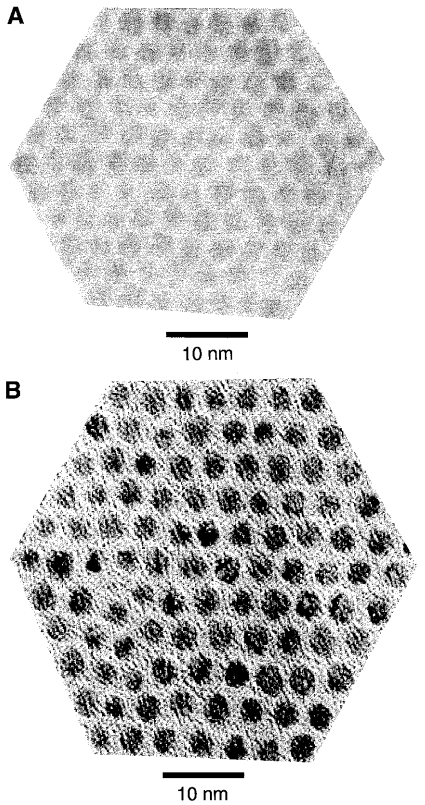

Fig. 2. TEM images of compressed films consisting of Ag particles, 27 Å in diameter, cropped so that each frame contains 102 particles. (**A**) Video capture image (exposure, 0.033 s) of hexanethiol-capped particles separated by ~6 Å. (**B**) Film image of decanethiol-capped particles separated by ~12 Å.

the maximum in the SHG signal corresponded to enhancement by a factor of ~500. The structure of the monolayer at any point of the isotherm can be inferred from the π-area curve. At the point where the pressure begins to rise, the monolayer is continuous, and barrier compression translates into decreasing the interparticle separation (the condensed, closest packed 2D phase of Fig. 1). Near 850 Å^2, the monolayer is incompressible, and further barrier compression leads to monolayer collapse (the collapsed phase of Fig. 1). After monolayer collapse, the film is again relatively compressible until the bilayer becomes continuous.

Because the SHG signal plotted in Fig. 3A has been normalized to the signal observed for an uncompressed monolayer, the increase in signal strength as the monolayer is compressed must originate from interparticle coupling. Two aspects of the SHG signal are important. The first is the large increase in the SHG signal as the monolayer is compressed. For an isotropic surface, pure s- or p-polarized radiation incident upon the surface will produce only p-polarized output (*28*). Thus, the use of s-polarized input and detection of p-polarized output constitutes a sensitive test for particle interactions in the plane of the monolayer. The material-dependent parameter, $|\chi^{(2)}|$, is simply the square root of the SHG signal. The change in $\chi^{(2)}$ as a function of interparticle separation can be fitted to the function exp(–*D*) (Fig. 3B). This is the functional form expected for the decay of a wave function in the presence of a central Coulombic potential. This fit implies that the SHG increase is related to the overlap of individual quantum dot wave functions. Because the measured interparticle separation distances are sufficiently close, wave function overlap should be important throughout the compressed region of the isotherm.

The second interesting feature of the data in Fig. 3A is the sudden decrease in the SHG signal that occurs well before monolayer collapse. This discontinuity apparently correlates with a particular interparticle separation distance, but not with some structural phase transition in the thin film. Langmuir films of 27 Å/C_{10} particles, which can be compressed to a minimum interparticle separation distance of ~10 Å, do not exhibit such behavior. The SHG generated from 27 Å/C_{10} monolayers exhibits only one-third as much enhancement upon film compression. It rises up to the point of monolayer collapse and then exhibits a gradual decrease as the compressed monolayer relaxes into the second layer. Langmuir monolayers of the 40 Å/C_3 particles behave similarly to the 27 Å/C_6 particles: $\chi^{(2)}$ rises exponentially (at a rate similar to that for the 27 Å/C_6 particles) upon compression, up to a particular interparticle separation distance, at which point $\chi^{(2)}$ decreases to a nearly constant value. One possible explanation for the sharp discontinuity in the SHG data for the 27 Å/C_6 and 40 Å/C_3 films is that the energy gain from electron delocalization becomes sufficient to overcome the site (single-particle) charging energy. This would correspond to an insulator-to-metal transition (*29, 30*).

If wave function overlap and insulator-metal transitions are occurring in some of these compressed monolayers, then the linear optical response should reflect this as well. The linear reflectance-absorption data (collected as functions of particle size, ligand length, and pressure) make up a complex data set, and only the most salient points are presented here. The various particle monolayers can be characterized by the parameter *D*/2*R*, where *D* is the separation between adjacent particle centers and 2*R* is the diameter of a particle. *D*/2*R* does not treat particle size independently and is thus an approximation. Nevertheless, the following description is a reasonably accurate summary of our findings.

Dilute solutions of particles are represented by some limiting large *D*/2*R* value. By compressing monolayers of the 27 Å/C_{10}, 27 Å/C_6, and 40 Å/C_3 particles, it is possible to vary *D*/2*R* nearly continuously from ~1.7 to 1.1. As *D*/2*R* is decreased from the limiting solution-phase value to 1.7 (an uncompressed, continuous film of 27 Å/C_{10} particles), ω_{sp} shifts from 2.8 to 2.55 eV. As *D*/2*R* decreases from 1.7 to 1.2, ω_{sp} shifts from 2.55 to 2.2 eV, and the reflectivity increases by more than a factor of 10. The "red shift" in ω_{sp} and the increased reflectivity as *D*/2*R* is decreased are both well described by a classical model that accounts for the changing local fields around a particle (*31*). Such a model predicts a continued shift to lower energies and an increasing optical reflectivity until *D*/2*R* reaches the limiting value of 1. Just below *D*/2*R* = 1.2, however, the trend is reversed; ω_{sp} shifts back to near 2.3 eV and the reflectivity drops sharply. A second experimental observation is the dependence of the linewidth (Γ) of ω_{sp} on *D*/2*R*. The classical model predicts very little change in Γ as *D*/2*R* decreases. We observe, however, that the linewidth narrows by as much as 30%. Line narrowing can be accounted for by a quantum coupling model that invokes electron delocalization over adjacent particles by wave function overlap. This same model also accounts for the observed exponential increase of $\chi^{(2)}$ with decreasing *D*/2*R*. The

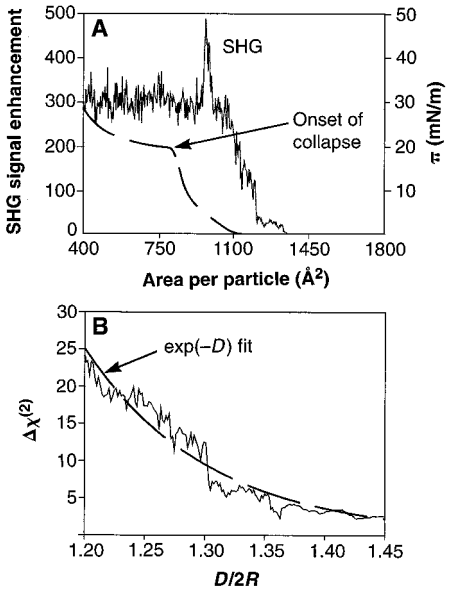

Fig. 3. (**A**) Surface pressure of the Langmuir film (π) and SHG signal enhancement as a function of area per particle for hexanethiol-capped particles. The SHG has been normalized to the signal observed from the uncompressed monolayer, indicating that the enhancement originates from interparticle coupling. (**B**) Change in $|\chi^{(2)}|$ versus *D*/2*R*, where *D* is the center-to-center particle separation distance and *R* is a particle radius. Also shown is a best fit of the curve exp(–*D*) to the data. The exponential behavior of $|\chi^{(2)}|$ is consistent with a quantum mechanical mechanism for interparticle coupling.

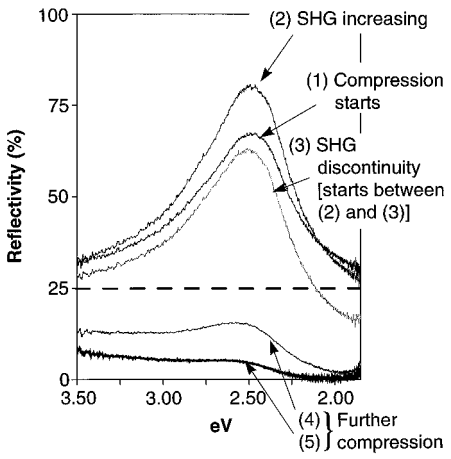

Fig. 4. Ultraviolet–visible reflectance spectra from a Langmuir monolayer of 40 Å particles passivated with *n*-propanethiol, collected in situ as the film was compressed. The dashed line corresponds to the reflectance of a clean water surface. Correlations with the nonlinear optical response are indicated. Below ~5 Å separation between particles, the reflectance spectra [(4) and (5)] begin to resemble that of a thin, metallic film. The decrease in reflectance and the disappearance of the strong surface plasmon resonance correspond to a discontinuity in the SHG signal similar to that shown in Fig. 3. All data were collected from an uncollapsed film, and the transition was reversible.

classical model, on the other hand, predicts a high-order polynomial dependence of $\chi^{(2)}$ on $D/2R$.

For $D/2R < 1.2$, there is a discontinuity in both the $\chi^{(2)}$ versus $D/2R$ trend and in the reflectance (absorbance) behavior versus $D/2R$. Several spectra collected from an uncollapsed Langmuir film of 40 Å/C_3 particles are shown in Fig. 4. Upon initial compression, the film becomes more reflective, as described qualitatively above. In this region, $\chi^{(2)}$ is increasing exponentially. At the point where the SHG data exhibit a discontinuity, the reflectance drops precipitously; in the near-infrared, it is below measurable levels. This decrease in reflectivity is accompanied by an equally large increase in absorptivity. The final reflectance spectrum is similar to that reported for thin, metallic silver films (*32*) and indicates that the Langmuir film has become metallic.

Our experimental data provide strong evidence for the onset of quantum mechanical coupling between adjacent silver nanocrystals when interparticle separation distances are reduced below 12 Å, and for a reversible insulator-to-metal transition when the particle separation distance is reduced below 5 Å. Our observations thus provide evidence of quantum mechanical coupling in quantum dot superlattices. In addition, this work constitutes an example of a reversible metal-insulator transition in a solid-state system (*33*) under ambient conditions. These results imply the possibility of fabricating a new class of solids, composed of metal quantum dots, in which the electronic band structure of the solid is "tailored" through the adjustment of electronic wave function overlap between adjacent particles.

REFERENCES AND NOTES

1. M. Brust *et al., J. Chem. Soc. Chem. Commun.* **1994**, 801 (1994).
2. N. Herron, J. C. Calabrese, W. E. Farneth, Y. Wang, *Science* **259**, 1426 (1993).
3. T. Vossmeyer *et al.*, *ibid.* **267**, 1476 (1995).
4. C. B. Murray, D. J. Norris, M. G. Bawendi, *J. Am. Chem. Soc.* **115**, 8706 (1993).
5. P. C. Ohara, D. V. Leff, J. R. Heath, W. M. Gelbart, *Phys. Rev. Lett.* **75**, 3466 (1995).
6. C. B. Murray, C. R. Kagan, M. G. Bawendi, *Science* **270**, 1335 (1995).
7. R. L. Whetten *et al., Adv. Mater.* **8**, 428 (1996).
8. R. P. Andres *et al., Science* **273**, 1690 (1996).
9. J. H. Fendler and F. C. Meldrum, *Adv. Mater.* **7**, 607 (1995).
10. R. G. Freeman *et al., Science* **267**, 1629 (1995).
11. Th. Förster, in *Comparative Effects of Radiation,* M. Burton, J. S. Kirby-Smith, J. L. Magee, Eds. (Wiley, New York, 1960), chap. 13.
12. D. L. Dexter, *J. Chem. Phys.* **21**, 836 (1953).
13. C. R. Kagan, C. B. Murray, M. G. Bawendi, *Phys. Rev. B* **54**, 8633 (1996).
14. C. R. Kagan, C. B. Murray, M. Nirmal, M. G. Bawendi, *Phys. Rev. Lett.* **76**, 1517 (1996).
15. C. A. Mirkin, R. L. Letsinger, R. C. Mucic, J. J. Storhoff, *Nature* **382**, 607 (1996).
16. For examples of relatively early work on optically probed percolation phenomena in granular metal materials, see R. W. Cohen, G. D. Cody, M. D. Coutts, B. Abeles, *Phys. Rev. B* **8**, 3689 (1973); E. B. Priestley, B. Abeles, R. W. Cohen, *ibid*. **12**, 2121 (1975).
17. D. Ricard, P. Roussignol, C. Flytzanis, *Opt. Lett.* **10**, 511 (1985).
18. C. F. Bohren and D. R. Huffman, *Absorption and Scattering of Light by Small Particles* (Wiley, New York, 1983); H. C. van de Hulst, *Light Scattering by Small Particles* (Wiley, New York, 1957); U. Kreibig and M. Vollmer, *Optical Properties of Metal Clusters* (Springer, Berlin, 1995).
19. T. Takagahara, *Surf. Sci.* **267**, 310 (1992).
20. ———, *Optoelectron. Dev. Technol.* **8**, 545 (1993).
21. Y. Kayanuma, *J. Phys. Soc. Jpn.* **62**, 346 (1993).
22. C. K. Chen, A. R. B. de Castro, Y. R. Shen, *Phys. Rev. Lett.* **46**, 145 (1981).
23. V. Kresin, *Phys. Rev. B* **38**, 3741 (1988).
24. J. R. Heath, C. M. Knobler, D. V. Leff, *J. Phys. Chem. B* **101**, 189 (1997).
25. Because of electron beam–induced particle instability, particle monolayers with $\delta < 8$ Å were difficult to image. For images of the 27 Å/C_6 particles, a previously unexposed portion of the TEM grid was quickly brought into view, and an image (exposure time, 0.033 s) was immediately captured.
26. Samples for TEM were prepared at UCLA and transported to the University of Southern California Center for Electron Microscopy. For this reason, films had to be stable for at least 2 hours or they could not be imaged. Compressed monolayers of 40 Å/C_3 particles did not exhibit sufficient stability.
27. SHG signals from static Langmuir monolayers were measured over time to ascertain whether the laser was damaging the monolayers. The signal was very stable for all time periods investigated (up to 20 min), and optical microscopic inspection of the illuminated spot revealed no evidence of film damage. Indeed, the monolayers could be redissolved in hexane after the experiments were carried out.
28. Y. R. Shen, *Annu. Rev. Phys. Chem.* **40**, 327 (1989).
29. N. F. Mott, *Metal-Insulator Transitions* (Taylor & Francis, London, 1990).
30. P. P. Edwards and M. J. Sienko, *Acc. Chem. Res.* **15**, 87 (1982).
31. I. Farbman and S. Efrima, *J. Phys. Chem.* **96**, 8469 (1992).
32. C. A. Davis, D. R. McKenzie, R. C. McPhedran, *Opt. Commun.* **85**, 70 (1991).
33. A second well-studied example would be the superconducting transition in high-T_c materials.

34. We thank G. Markovich and S.-W. Chung for help in particle synthesis. Supported by the NSF–National Young Investigator program and by the Office of Naval Research, order N00014-95-F-0099, under the auspices of the ONR-funded Molecular Design Institute at UC Berkeley (J.J.S., S.E.H., J.R.H.), fellowships from the Packard Foundation and the Sloan Foundation (J.R.H.), and NSF grant CHE-9424482 (C.P.C. and R.J.S.).

3 April 1997; accepted 11 August 1997

Regioselective Stepwise Growth of Dendrimer Units in the Internal Voids of a Main Dendrimer

Christophe Galliot, Christophe Larré, Anne-Marie Caminade,* Jean-Pierre Majoral*

Dendrimers constitute a class of polymers with unique properties and applications resulting from the presence of internal voids and of a large number of functionalities on the surface. The development of a macromolecular chemistry within the cavities of dendrimers is illustrated here. Two examples of construction of six dendrimer units within the cascade structure of a main dendrimer are reported. The preparation of these multidendritic systems involves the regioselective modification of the framework of the central dendrimer to create internal reactive centers, followed by the stepwise synthesis of the six dendritic macromolecules.

During the past decade, there has been an explosive growth in studies of dendrimers, a new class of macromolecules that can be considered as monodisperse, precisely ordered polyfunctional polymers. Several applications of these relatively soluble compounds have been proposed (*1*). Their remarkable properties result from the presence of a large number of chain-end functionalities that provide highly controlled surfaces and interfaces, and from the presence of internal voids allowing, for example, encapsulation of guest molecules (*2*) or molecular recognition at specific locations on the cascade superstructure (*3*).

A number of creative approaches to the synthesis of organic or inorganic "monodendrimers" have been reported (*1*). The reactivity of the core has been used to couple two or more dendrons leading, for example, to structures with two dissimilar halves (*4*). Coupling of cascade macromolecules through metal centers has also been achieved (*5*). Dendrons containing isophthalic acid units covalently attached to a rigid aromatic spacer have been shown to self-assemble through hydrogen bonding to form a hexameric dendritic aggregate whose stability varies in a generation-dependent manner (*6*). All these different routes to bis- or multidendrimers (*7*) involve the association of dendrons by their core.

An alternative way to build multidendritic systems is based on the use of internal functional groups of a dendrimer. To apply such a concept, it is first necessary to

Laboratoire de Chimie de Coordination, CNRS, 205 route de Narbonne, 31077 Toulouse Cedex 4, France.

*To whom correspondence should be addressed. E-mail: majoral@lcctoul.lcc-toulouse.fr